Neutron diffraction and magnetic properties of $Co_2Cr_{1-x}Ti_xAl$ Heusler alloys

Priyanka Nehla,[1] Yousef Kareri,[2] Guru Dutt Gupt,[1] James Hester,[3] P. D. Babu,[4] Clemens Ulrich,[2] and R. S. Dhaka[1,*]

[1]*Department of Physics, Indian Institute of Technology Delhi, Hauz Khas, New Delhi-110016, India*

[2]*School of Physics, The University of New South Wales, Kensington, 2052 NSW, Sydney, Australia*

[3]*Australian Centre for Neutron Scattering, Australian Nuclear Science and Technology Organisation (ANSTO), New Illawarra Road, Lucas Heights NSW 2234, Australia*

[4]*UGC-DAE Consortium for Scientific Research, Trombay, Mumbai-400085 India*

(Received 17 September 2019; published 30 October 2019)

We report the structural, magnetic, and magnetocaloric properties of $Co_2Cr_{1-x}Ti_xAl$ ($x = 0$–0.5) Heusler alloys for spintronic and magnetic refrigerator applications. Room-temperature x-ray diffraction and neutron diffraction patterns along with Rietveld refinements confirm that the samples are of single phase and possess a cubic structure. Interestingly, magnetic susceptibility measurements indicate a second-order phase transition from paramagnetic to ferromagnetic where the Curie temperature (T_C) of Co_2CrAl increases from 330 K to 445 K with Ti substitution. Neutron powder diffraction data of the $x = 0$ sample across the magnetic phase transition taken in a large temperature range confirm the structural stability and exclude the possibility of antiferromagnetic ordering. The saturation magnetization of the $x = 0$ sample is found to be 8000 emu/mol (1.45 μ_B/f.u.) at 5 K, which is in good agreement with the value (1.35 ± 0.05 μ_B/f.u.) obtained from the Rietveld analysis of the neutron powder diffraction pattern measured at a temperature of 4 K. By analyzing the temperature dependence of the neutron data of the $x = 0$ sample, we find that the change in the intensity of the most intense Bragg peak (220) is consistent with the magnetization behavior with temperature. Furthermore, an enhancement of change in the magnetic entropy and relative cooling power values has been observed for the $x = 0.25$ sample. Interestingly, the critical behavior analysis across the second-order magnetic phase transition and extracted exponents ($\beta \approx 0.496$, $\gamma \approx 1.348$, and $\delta \approx 3.71$ for the $x = 0.25$ sample) suggest the presence of long-range ordering, which deviates toward 3D Heisenberg-type interactions above T_C, consistent with the interaction range value σ.

DOI: 10.1103/PhysRevB.100.144444

I. INTRODUCTION

Heusler alloys are intermetallic compounds with the general formula X_2YZ for full- and XYZ for half-Heusler compounds, where X and Y are transition-metal elements and Z represents an *sp* element like Al, Ga, Si, or another main group metal [1]. Interestingly, the $Co_2Cr_{1-x}T_xZ$ (T = transition metal) Heusler alloys are considered potential candidates for various practical applications, as these materials have theoretically been predicted to be half-metallic ferromagnets (HMFs) with 100% spin polarization [2–4], and possess excellent structural stability, low magnetic damping [5], anomalous Hall conductivity [6], large negative magnetoresistance [7] as well as a high Curie temperature (T_C) above room temperature [8,9]. These are most favorable properties for the technological development of spintronic devices operating at and above room temperature [1]. However, understanding the role of temperature/field dependence of the magnetic properties and local atomic ordering [9–12] is crucial in making real use of these materials in device applications [13]. In general, the Co_2-based Heusler alloys possess the fully ordered $L2_1$ structure and the experimentally determined magnetic moment is in agreement with the theoretical calculated value using the Slater-Pauling (SP) rule [9,14,15]. Disorder can transform the $L2_1$ structure to B2 type (disorder between Y and Z atoms) or A2 type (disorder between X, Y, and Z atoms). In case of the Co_2CrAl alloy, the increasing Co-Cr type disorder [12,16,17] can drastically reduce the spin polarization and therefore the total magnetic moment due to an antiferromagnetic coupling of the antisite Cr with the first-nearest-neighbor ordinary-site Cr and Co atoms [18,19]. With this respect, using powder neutron-diffraction (ND) technique, Mukadam *et al.* quantified the site disorder and studied its effect on the spin polarization of the NiFeMnSn Heusler alloy, which is predicted to show nearly half-metallic nature in band-structure calculations [20]. Therefore, the role of disorder between X, Y, and Z atoms is of crucial importance to control the magnetic moment, the half metallicity, and the spin polarization in Heusler alloys [16,17,19,21].

On the other hand, Kandpal *et al.* showed that antisite disorder of 10–12% between Co/Ti does not change the half-metallic character and magnetization in Co_2TiSn [22]. Moreover, first-principles calculations demonstrated that Co_2TiZ alloys are half metallic and ferromagnetic (FM) in nature even when the Z element is from the III, IV, or V group. However, it was suggested that disorder between Ti/Al reduces the half metallicity [23]. One of the most favorable properties of these Heusler alloys for potential future applications is the fact that they offer a direct tunability of their electronic and magnetic properties [24–26] through the substitution of one of the transition metals with another element. Interestingly, the

*rsdhaka@physics.iitd.ac.in

magnetic properties of $Co_2Cr_{1-x}Ti_xAl$ Heusler alloys show a decrease in the total magnetization and the sample with $x = 0.5$ possesses the most stable half metallicity [24]. Feng and Xu reported that with increasing Ti concentration, the Fermi level shifts from the bottom to top of the minority spin gap and is located in the middle of the gap for a Ti concentration of $x = 0.5$ [24]. Therefore, the effect of substitution in the ternary Heusler alloys opens the gate to discover new materials [6,27,28] and hence the understanding of the physical properties is vital for their practical applications.

In recent years, tremendous research interest has also been generated in Heusler alloys due to their magnetocaloric properties, which offer a large potential for applications in magnetic refrigerators [29,30]. It is important to note that magnetic refrigeration has advantages over compression/expansion techniques due to their low cost, highly efficient, and, most importantly, environment friendly operation since no compressor/refrigerator gas is required [31]. Therefore, the scientific interest in materials with magnetic cooling near room temperature has grown significantly. For example, compounds with the rare-earth element Gd have a large magnetocaloric effect (MCE) and have been actively investigated for use in magnetic refrigerators [31]. In particular, intermetallic compounds such as Gd-Si-Ge, Mn-Fe-P-Si, and La-Fe-Si [32] were found to be highly efficient. However, at the same time, rare-earth materials are very expensive. An alternative to rare-earth compounds, the transition-metal-based magnetocaloric materials, in particular Heusler alloys, are one of the suitable candidates for magnetic refrigeration near room temperature because of their large MCE and the adiabatic temperature change [33]. Of particular interest are Ni-based alloys since they show a first-order magnetic phase transition and a large magnetic entropy change within a small temperature range [33]. However, under an applied magnetic field and temperature variation, they exhibit large thermal and magnetic hysteresis, which limits their use for practical applications. A few Ni-Mn-based materials have already been explored [33], which show giant MCE, but they are not suitable for practical application because of their thermal and magnetic hysteresis, which are detrimental to the refrigerant capacity [34]. In this regard, a few studies have reported on second-order magnetic phase transition materials which exhibit a large change in the magnetic entropy [34–36]. On the other hand, the Co-based Heusler alloys remain largely unexplored for this purpose [25,30]. Therefore, it is desirable to search for new materials which exhibit large MCE and negligible thermal and magnetic hysteresis with a second-order magnetic phase transition.

In this investigation, we have studied the structural, magnetic, and magnetocaloric properties of $Co_2Cr_{1-x}Ti_xAl$ Heusler alloys with Ti concentrations of $x = 0$, 0.25, and 0.5. Using Rietveld refinements of powder x-ray diffraction (XRD) and powder ND patterns we were able to confirm that the samples possess a stable single phase with a cubic crystal structure. Interestingly, we observe a second order magnetic phase transition from the paramagnetic (PM) to the FM state where the Curie temperature can be tuned with Ti substitution from 330 K ($x = 0$ sample) to 445 K for the $x = 0.5$ sample. This property makes these materials extremely useful for technological applications. The saturation magnetization of the $x = 0$ sample is found to be 8000 emu/mol (1.45 μ_B/f.u.), which is in good agreement with the value of 1.35 ± 0.05 μ_B/f.u. extracted by the Rietveld analysis of ND pattern measured at 4 K. The analysis of the temperature-dependent ND data of the $x = 0$ sample shows that the change in the magnetic intensity of the most intense Bragg peak (220) is consistent with the magnetization behavior with temperature. We found a conventional MCE across the PM-FM phase transition and the $x = 0.25$ sample shows the highest ΔS_m and relative cooling power (RCP) values at 9 T. More interestingly, using critical behavior analysis across the second-order magnetic phase transition for the $x = 0.25$ sample, the obtained exponent $\beta \approx 0.496$ suggests the presence of long-range ordering below T_C, which deviates from mean field toward 3D Heisenberg-type interactions above T_C where the exponents are $\gamma \approx 1.348$ and $\delta \approx 3.71$ [37].

II. EXPERIMENTAL DETAILS

Polycrystalline $Co_2Cr_{1-x}Ti_xAl$ (x =0, 0.25, 0.5) samples have been synthesized from high purity (>99.99%) elements Co, Cr, Ti, and Al from Alfa Aesar and/or Sigma Aldrich. An arc furnace from Centorr vacuum industries, USA, was used to prepare an ingot by melting the stoichiometric amount of the starting materials on a water-cooled Cu hearth in an argon atmosphere. To improve the homogeneity, the ingot was flipped and melted 4–5 times. The loss in weight was less than 1% after the melting process. Further, we wrapped the ingot in a Mo foil and sealed it in a quartz tube under vacuum for the final annealing at 575 K for 10 days. To determine the quality of the obtained samples, powder XRD measurements were performed at room temperature on a Panalytical diffractometer using the Cu Kα (λ = 1.5406 Å) radiation. Magnetization measurements were performed using a physical property measurement system from the company Quantum Design, USA. Neutron powder-diffraction experiments have been performed using the high-intensity neutron diffractometer WOMBAT [38] and the high-resolution diffractometer ECHIDNA [39,40] at the OPAL research reactor at ANSTO, Australia. At the high-intensity diffractometer WOMBAT, a wavelength of $\lambda = 1.633$ Å was selected using a Ge(113) monochromator. Scans at various temperatures were recorded on heating from the base temperature of around 4 K up to a temperature well above the magnetic phase transition. In addition, diffraction patterns were collected at selected temperatures above and below the magnetic phase transition on the high-resolution diffractometer ECHIDNA using a wavelength of $\lambda = 1.622$ Å obtained by a Ge(335) monochromator. The measured diffraction patterns were analyzed with the Rietveld refinement method using the FULLPROF package [41].

III. RESULTS AND DISCUSSION

The powder XRD patterns of the $Co_2Cr_{1-x}Ti_xAl$ ($x = 0$, 0.25, 0.5) samples were measured at room temperature, which are shown in Figs. S1(a)–S1(c) of Ref. [42] together with the Rietveld refinement profiles. We observe Bragg peaks corresponding to the (200), (220), (400), and (422) planes only, which indicates a cubic structure for all these samples. The absence of additional peaks confirms the phase purity of the samples and the absence of the (111) reflection indicates

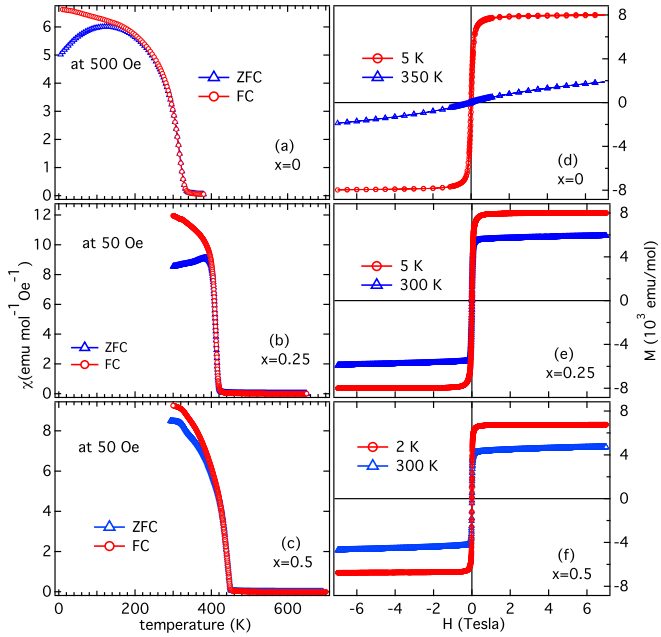

FIG. 1. (a)–(c) The variation of magnetic susceptibility (χ) with temperature and (d)–(f) isothermal magnetization M of $Co_2Cr_{1-x}Ti_xAl$ ($x = 0, 0.25, 0.5$) samples.

a B2-type ordering in these samples, i.e., Cr and Al may partially exchange their atomic positions. Usually the presence of the (200) reflection confirms the ordering of the Co sublattice; however, due to the similar x-ray scattering cross-sections of Co (0.24) and Cr (0.27) [43], no firm conclusion can be drawn about the local disorder between the two elements, which plays crucial role for the determination of the magnetic moment. On the other hand, theoretical calculations have predicted that the perfectly ordered $L2_1$ structure is more stable in Co_2CrAl [16]. We have performed Rietveld refinements of the XRD patterns using the $Fm\bar{3}m$ (No. 225) space group where the background has been fitted by linear interpolation between the experimental data points. The refinements provide reasonably good fits to the experimental data by assigning the Wyckoff positions (1/4, 1/4, 1/4), (0, 0, 0), and (1/2, 1/2, 1/2) to the Co, Cr/Ti and Al atoms, respectively. For the $x = 0$ sample, the lattice parameter a obtained from the refinement is found to be 5.742 Å, which is consistent with the reported value 5.726 Å [17]. For both Ti substituted samples ($x = 0.25$, 0.5), the lattice parameter a increases to ≈5.816 Å. Note that the reported value of the lattice parameter a for Co_2TiAl is 5.849 Å [27]. The change in the lattice parameter is consistent with the increase in the atomic radius from Cr (128 pm) to Ti (147 pm), which results in the expected increase of the total unit cell volume (a^3) of $Co_2Cr_{1-x}Ti_xAl$ with the corresponding Ti concentration at the Cr site.

The magnetic susceptibility (χ) measured as a function of temperature in zero-field-cooled (ZFC) and field-cooled (FC) protocols are shown in Figs. 1(a)–1(c) for $Co_2Cr_{1-x}Ti_xAl$ ($x = 0$–0.5) samples. For the $x = 0$ sample, the magnetic phase transition is at $T_C \approx 330$ K, which is in good agreement with the value reported in Ref. [6]. An important result is the fact that T_C increases from 330 K to 410 K for the $x = 0.25$ sample and further to 445 K for the $x = 0.5$ sample. On the other hand, T_C of Co_2TiAl has been reported to be about 120 K [28]. The partial substitution of Cr with Ti enhances T_C significantly above room temperature, which make these materials extremely useful for practical applications in spintronics and magnetic refrigerators. The smooth behavior and the absence of a thermal hysteresis at the phase transition (data not shown here) from the PM to the FM state are indications of a second-order phase transition in these samples. Figures 1(d)–1(f) show the variation of magnetization with applied magnetic field at constant temperature, which indicates the soft FM nature of these samples. There is no significant change in the total magnetization [8000 emu/mol (1.45 μ_B/f.u.) at 5 K] between the $x = 0$ and 0.25 samples [Figs. 1(d) and 1(e)]. The isothermal magnetization of the $x = 0.25$ sample shows a FM nature at 300 K. On the other hand, the magnetization of $x = 0.5$ sample decreases to about 7000 emu/mol (1.25 μ_B/f.u.), see Fig. 1(f). We note that in the present case, the magnetic moment of the $x = 0$ sample is significantly lower than the calculated value of 3 μ_B as per the SP rule (given by $M_t = Z_t - 24$, where M_t is the total spin magnetic moment per f.u. in μ_B and Z_t is the total number of valence electrons [2]), if we consider the sample in a fully ordered state [45]. On the other hand, the experimental value of the magnetic moment has been reported to be in the range of 1.5 to 3 μ_B/f.u. for Co_2CrAl [17,44,45].

Block *et al.* performed band-structure calculations and reported that the magnetic moments are mainly localized at the Co (≈0.8 μ_B) and Cr (≈1.6 μ_B) sites. This indicates a FM interaction between the transition metals (Co and Cr) and, as a consequence, the formation of the energy gap of about 0.2 eV in the minority bands [45]. It has also been suggested that the experimentally observed lower value of the magnetic moment in Co_2CrAl can be influenced by the local structural antisite disorder between Co and Cr, which might introduce a local antiferromagnetic ordering [19].

The total number of valence electrons change from 27 in Co_2CrAl to 25 in Co_2TiAl. Therefore, the SP behavior predicts that the saturation magnetic moment should decrease with the partial substitution of Ti at the Cr site, i.e., 2 μ_B for $Co_2Cr_{0.5}Ti_{0.5}Al$ and 1 μ_B for Co_2TiAl. Recently, Mizusaki *et al.* used magnetic Compton scattering and reported a value of the moment of about 1.5 μ_B and 1 μ_B for Co_2CrAl and Co_2TiAl, respectively [26]. The lower value of the magnetic moment may be due to constant $sp - d$ magnetic interactions in Co_2CrAl [26]. Also, the existence of an orbital moment of the Co ions has been suggested [46,47]. For example, an orbital moment of −0.15 μ_B/f.u. has been attributed to the Co ions in the Co_2TiAl Heusler alloy [46,47]. In the present case, we observe a value of the moment of about 1.25 μ_B/f.u. for the $x = 0.5$ sample, which is still lower than the SP behavior (2 μ_B/f.u.). Interestingly, it has been reported that the Co–Cr(Ti)-type disorder in Co_2CrAl alloys significantly reduces the spin polarization, but not the Cr(Ti)–Al-type disorder [19]. Therefore, it becomes important to determine the type of disorder in this Heulser alloy. In general, one can get an idea about the degree of disorder in X_2YZ Heusler alloys by taking the intensity ratio of (111) and (200) peaks, conventional XRD cannot give accurate results as nearby elements in the periodic table have almost the same value of atomic scattering amplitude [48]. Note that in our

case, (Co_2CrAl), the x-ray scattering amplitudes of Co and Cr are nearly same, which makes it difficult to perform a quantitative analysis of the disorder using conventional XRD. However, due to the different scattering amplitudes, ND is more sensitive to the antisite disorder as compared to the x-ray diffraction. Also, neutron study can help if there is antiferromagnetic/ferrimagnetic alignment [49] of the Co and Cr spins, which may explain the lower experimental value of the magnetic moment in Co_2CrAl. For example, the ND measurements show a ferrimagnetic alignment between two different Mn atoms present in Mn_2VGa [50]. Therefore, it is vital to perform ND measurements on the Co_2CrAl Heusler alloy across the magnetic phase transition in a large temperature range [51].

To understand the local atomic ordering and magnetic behavior, we have carried out neutron powder-diffraction measurements across the magnetic phase transition temperature of Co_2CrAl. We first used the high-resolution diffractometer ECHIDNA and performed measurements at a sample temperature of 400 K, 300 K, and 170 K. The corresponding diffraction pattern is presented in Figs. S2(a)–S2(c) of Ref. [42] along with the corresponding Rietveld refinements. The absence of the (111) Bragg reflection at all temperatures indicates the B2 structural order in the sample, which suggests disorder between the Cr and Al atoms. As discussed before, the measured total magnetic moment of the $x = 0$ sample (1.45 μ_B/f.u.) from the magnetization measurements is significantly lower than predicted from the SP rule (3 μ_B). However, disorder between Cr and Al is not expected to decrease the magnetic moment of Co-based Heusler alloys [19]. Here the lower value of the experimental magnetic moment can possibly be attributed to a certain type of disorder (between Co and Cr) in the system due to ferrimagnetic or antiferromagnetic spin alignment [16]. The Rietveld refinement of the ND pattern taken at 400 K, i.e., above T_C [see Fig. S2(c) of Ref. [42]], shows that the sample has a single cubic phase with the space group $Fm\bar{3}m$ and the refined lattice constant was found to be 5.708 Å. To determine the disorder between the Cr and Al atoms, the occupancies have been refined in such a way that the partial occupancy of Cr on Al site and Al on Cr site fulfill the condition that the total occupancy of atoms is conserved on both sites. However, since the neutron-scattering amplitudes of Cr (3.6 fm) and Al (3.5 fm) are almost identical, no conclusive result could be obtained about the Y–Z type disorder [43]. On the other hand, the neutron-scattering cross section is different for the Co (2.5 fm) and Cr (3.6 fm). Therefore, next we have introduced a disorder between Co and Cr atoms; however, no improvement in the refinement parameters was achieved. This suggests the absence of a disorder between Co and Cr for the $x = 0$ sample, which is expected as the presence of the (200) reflection in XRD/ND patterns rule out this possibility. Neutron diffraction of Co_2MnSi Heusler alloys shows no antisite disorder between Mn and Si; however, about 10% antisite disorder was found between Co and Mn in arc-melted samples [52].

The neutron powder-diffraction pattern taken at 170 K, i.e., at a temperature well within the magnetically ordered state, does not show additional Bragg reflections [see Fig. S2(a) of Ref. [42]]. This rules out the presence of an antiferromagnetic spin structure and points toward a ferro or ferrimagnetic structure [20,50]. In the present case, we observe only a slight increase in intensity of the Bragg peaks at 170 K as compared to 400 K. This makes it difficult to refine the diffraction pattern measured at 170 K with a magnetic phase and extract useful information about the magnetic structure [53]. A simulation with the magnetic moment determined by magnetization measurements did indicate that the slight increase in the Bragg peak intensities is in agreement with expected FM structure. However, the change in the Bragg peak intensity due to thermal effects, i.e., the Debye-Waller factor would give a similar change. Therefore, a more detailed analysis of the data is required. To detect distinct changes in the diffraction pattern across the magnetic phase transition temperature, we have used the high-intensity diffractometer WOMBAT to record the data in a large temperature range across the magnetic phase transition. Figure S3 of Ref. [42] shows the ND patterns of the $x = 0$ sample measured at temperatures from 4 K to 531 K. At first glance, no obvious change is present in the diffraction pattern apart from the expected shift of the Bragg peaks toward lower 2θ value with increasing sample temperature, which can be attributed to the thermal expansion of the material.

We have performed Rietveld refinements using the $Fm\bar{3}m$ space group for all temperatures, as shown in Fig. 2 for selected temperatures. The magnetization measurements show an increase in the magnetic moment below $T_C = 330$ K [see Fig. 1(a)]. The intensity of nuclear Bragg reflections should increase below T_C in the case of ferro- or ferrimagnetic ordering. Therefore, we have included a FM structure in the Rietveld refinements of the diffraction pattern measured below the transition temperature. The refinement parameters for the pattern taken at 4 K are $\chi^2 = 3.5$, Bragg R-factor = 2.45, RF-factor = 1.68, and magnetic R-factor = 8.21, which confirms the high quality of the fits [54]. The obtained value of total magnetic moment is 1.35 ± 0.05 μ_B, which is close to the value of 1.45 μ_B observed in M–H magnetization measurements, see Fig. 1(d), but is significantly lower than expected from the SP rule. This motivates for future investigation of these alloys using x-ray magnetic circular dichroism to understand the complex magnetic interaction and any possibility of orbital contribution. The ND data at each temperature have been fitted using Rietveld refinement and the obtained lattice parameter a is plotted as a function of sample temperature in Fig. 3(a). Further analysis reveals that the lattice constant increases with the square power of the temperature below ≈ 350 K while exhibiting an essentially linear behavior for higher temperatures. The change in the lattice parameter a follows the expected behavior for thermal expansion, which follows the Bose-Einstein statistics. The obtained constants from the fitting are: a1 = 5.6919 Å, b1 = 1.08 Å/K^2, a2 = 5.6854 Å, and b2 = 5.4192×10^{-5} Å/K. The calculated value of thermal coefficient is found to be 0.989×10^{-5}/K, which is consistent with Ref. [55]. A slight difference in a value extracted at room temperature from the XRD and neutron data analysis may be due to the fact that the XRD data have been measured with laboratory source having relatively poor resolution and other limitations of sample centering and zero calibration as compared to the neutron data. This further motivates us to perform synchrotron-based XRD measurements with better resolution and statistics.

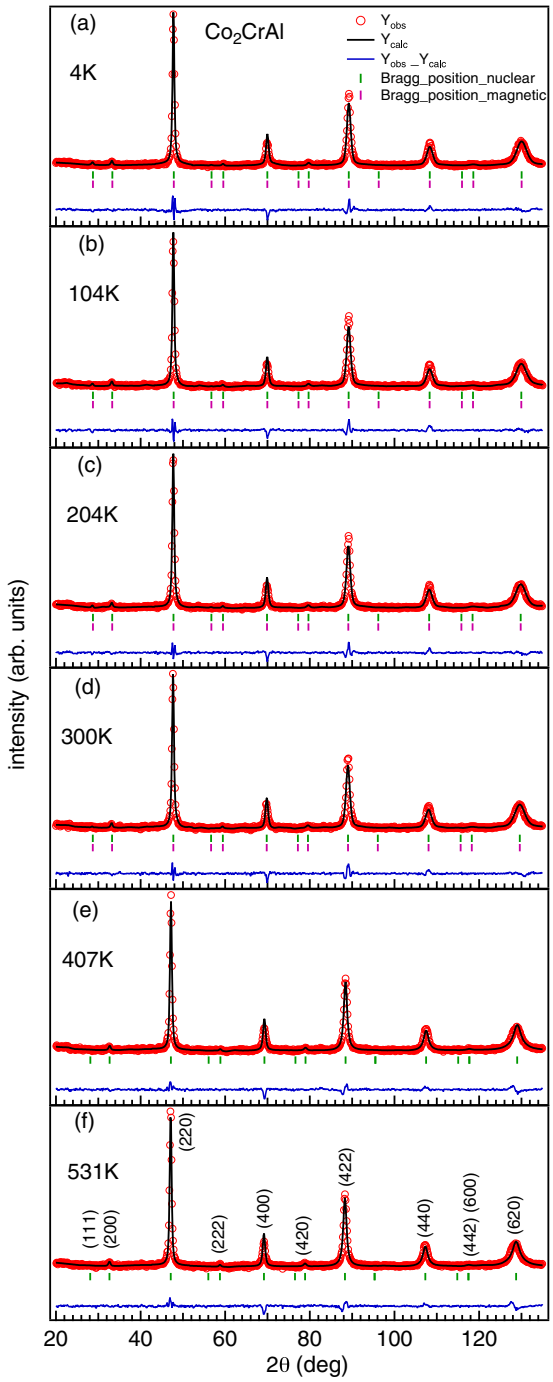

FIG. 2. The Rietveld refined neutron-diffraction data at selected temperatures of the $x = 0$ sample measured at the high-intensity defrectometer WOMBAT.

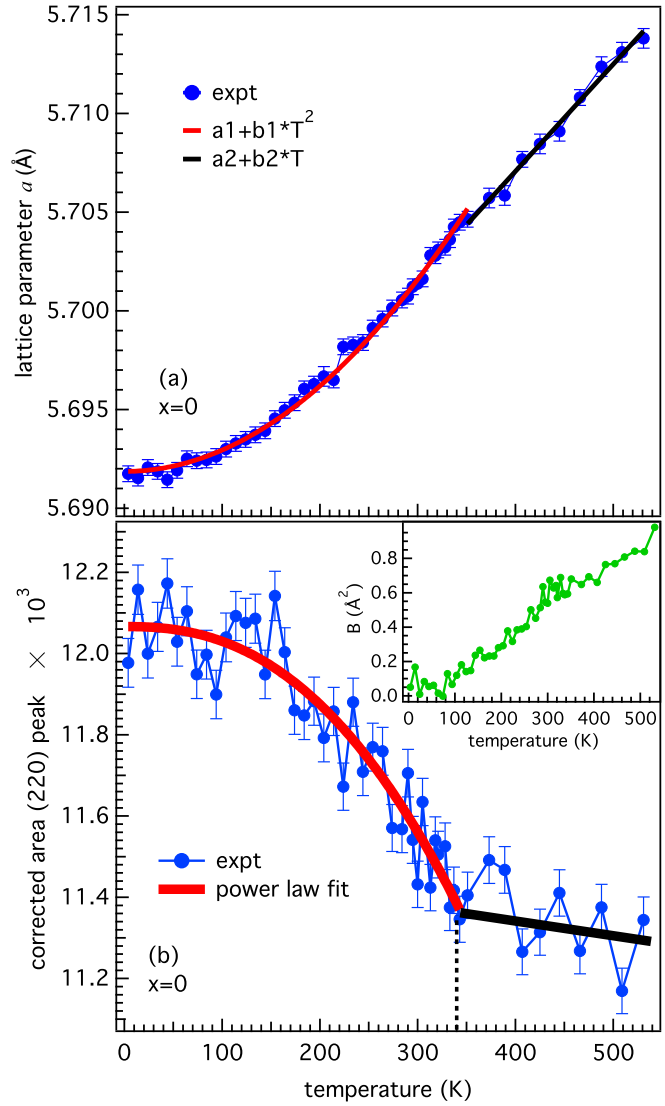

FIG. 3. (a) Variation in lattice constant a and (b) corrected intensity/area of the (220) peak with temperature for the $x = 0$ sample from the neutron-diffraction data measured at the high-intensity instrument WOMBAT. Inset in (b) shows the calculated B parameter with sample temperature.

To determine the magnetic contribution of the Bragg peak intensity, we have plotted the total area under the most intense (220) reflection peak (I_{220}) with temperature (not shown). Upon decreasing temperature, the intensity I_{220} is fairly constant down to the magnetic phase transition and then increases as the sample goes from the PM to the FM state. This behavior is consistent with the temperature dependence of the magnetization [Fig. 1(a)] and with the reported behavior on similar Heusler alloys [20]. Note that the moment of the $x = 0$ sample is quite weak and the magnetic phase transition takes place at a relatively high temperature where thermal effects can influence the intensity of the Bragg peaks as well. Therefore, it is important to determine the effect of temperature on the structural Bragg peaks, which is defined by the Debye-Waller parameter B. The magnetic structure factor decreases with 2θ and the Bragg peak at highest 2θ (=130°) has no significant magnetic contribution and its temperature dependence can be attributed to thermal effect only. To calculate the B parameter, the intensity of (620) Bragg peak ($2\theta = 130°$) at a particular temperature is expressed as [56] $I_{620}(T) = I_0 \times \exp(-2B\sin^2\theta/\lambda^2)$, where θ is the diffraction angle, λ is the wavelength of the x-ray/neutron source, and I_0 is the intensity when there are negligible thermal vibrations in the atoms at low temperatures (4 K in the present case). We assumed that the value of B is 0.05 Å^2 at 4 K, which is

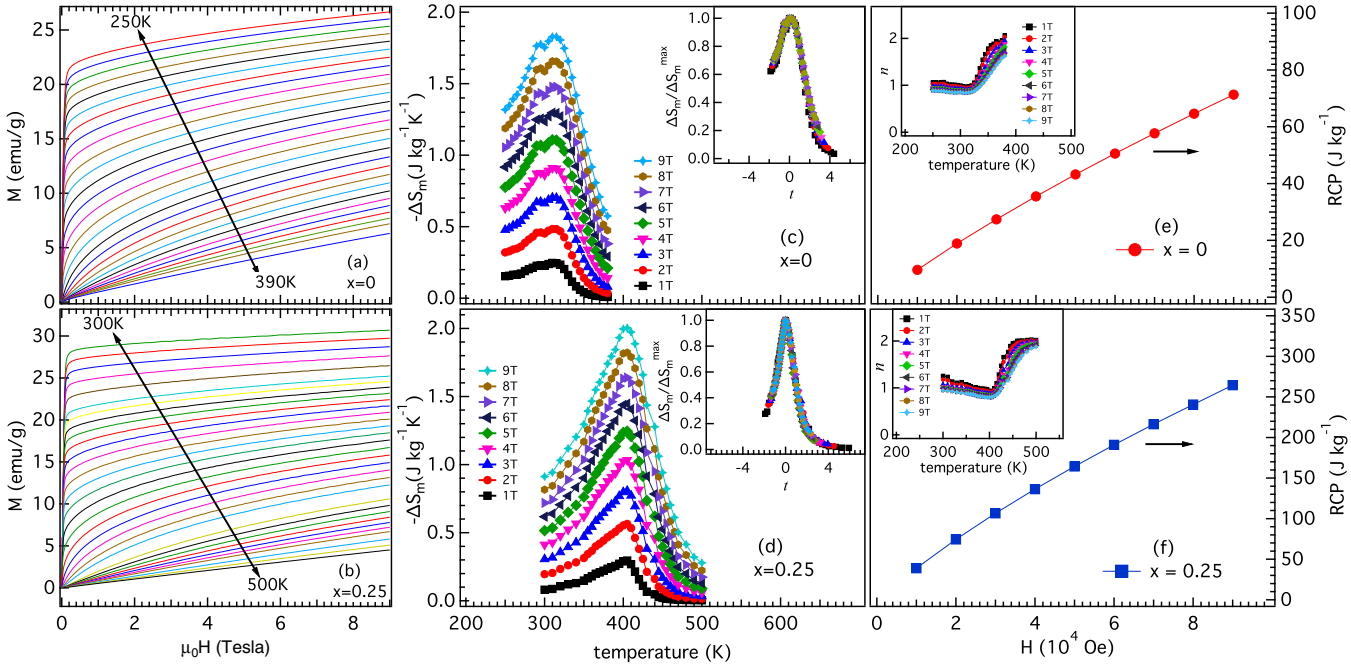

FIG. 4. (a), (b) Isothermal magnetization measured at various temperatures across the Curie temperature; (c), (d) change in the magnetic entropy ΔS_m with temperature; (e), (f) variation of the relative cooling power (RCP) with magnetic field for the $Co_2Cr_{1-x}Ti_xAl$ samples with $x = 0$ and 0.25. The insets in (c) and (d) are the normalized change in entropy with scaled temperature (t). The insets in (e) and (f) show the variation of exponent $n = d(ln|\Delta S_m|)/d(lnH)$ with temperatures at various magnetic fields.

reasonable as there are still quantum mechanical zero point vibrations present at temperature close to 0 K. The calculated values of B (using above equation) parameter, as shown in the inset of Fig. 3(b) as a function of sample temperature. These values of B were used to calculate corrected intensity of the (220) Bragg peak at each temperature as shown in Fig. 3(b). The intensity increases below the magnetic phase transition temperature 330 K and follows the increase in magnetic moment where the magnetic neutron-scattering intensity is proportional to M^2 [57,58].

To study the MCE in these materials, we have measured the isothermal magnetization for the $Co_2Cr_{1-x}Ti_xAl$ ($x = 0$, 0.25) samples in the vicinity of their respective magnetic phase transition temperature T_C [see Figs. 4(a) and 4(b)]. The Maxwell's equation $\Delta S_m = \int_0^H [\delta M(H,T)/\delta T]_H dH$ was used to extract change in the magnetic entropy (ΔS_m) from these isothermal magnetization curves. Figures 4(c) and 4(d) show ΔS_m versus sample temperature in the vicinity of T_C for magnetic fields from 1 T to 9 T. For the $x = 0$ and 0.25 samples, the temperature corresponding to the maximum in the entropy ΔS_m^{max} (T_{pk}) is close to T_C as observed in Figs. 1(a) and 1(b). Moreover, the measured $|\Delta S_m|$ value is about 2.0 J kg^{-1} K^{-1} at 9 T for the $x = 0.25$ sample. A comparable value of $|\Delta S_m| = 2.55$ J kg^{-1} K^{-1} was reported for the Co_2CrAl sample [30]. It is important to determine the precise magnetic interactions in $Co_2Cr_{1-x}Ti_xAl$ samples. Therefore, we have used the MCE curves for further analysis. First, to examine the field dependence of the experimental $|\Delta S_m|$ data at different magnetic fields, the value of a local exponent n can be calculated as $n = d(ln|\Delta S_m|)/d(lnH)$ [59], which depends on magnetic field and temperature. In the insets of Figs. 4(e) and 4(f), we show the plot of exponent n across the magnetic phase transition for the $x = 0$ and 0.25 samples, respectively. Note that below T_C, the value of n is ≈1, which decreases slightly at T_C and then increases up to 2 above T_C in the PM region [60]. However, we have observed that the value of n does not reach 2/3 at T_C, as predicted, if the system follows only the mean-field model. This suggests deviation from the mean-field-type interactions in these samples. Moreover, various theoretical studies associate $\Delta S_m(T)$ as a function of scaled temperature with a second-order phase transition for a ferromagnetic system [31,61–65]. Here the scaled temperature, t, is defined as follows [61,66]:

$$t = \begin{cases} -(T - T_{pk})/(T_{r1} - T_{pk}); & T \leqslant T_C \\ (T - T_{pk})/(T_{r2} - T_{pk}); & T > T_C, \end{cases} \quad (1)$$

where T_{r1} and T_{r2} are the reference temperatures below and above the magnetic phase transition temperature, respectively, which correspond to certain f ($= \Delta S_m(T)/\Delta S_m^{max}$) values, i.e., $\Delta S_m(T)/\Delta S_m^{max}$ versus t. T_{pk} is the temperature related to the maximum of ΔS_m. The temperatures T_{r1} and T_{r2} have been calculated using $f = 0.8$ and 0.5 for the $x = 0$ and 0.25 samples, respectively. It has been demonstrated that $\Delta S_m(T)/\Delta S_m^{max}$ versus scaled temperature for different applied magnetic fields overlap into one single curve [64,65], as shown in the insets of Figs. 4(c) and 4(d) for the $x = 0$ and 0.25 samples. This is a universal behavior of the MCE for ferromagnetic materials with a second-order phase transition.

The RCP is a further important parameter for the suitability of these alloys as magnetocaloric materials, where a high value is favorable for refrigeration applications. The $Co_2Cr_{1-x}Ti_xAl$ Heusler alloys have the benefit to possess high RCP values due to their broad second-order phase transition

at high temperatures. The RCP can be calculated by taking the product of the maximum entropy change and the temperature range of the full width half maximum, i.e., RCP $= |-\Delta S_m| \times \delta T_{\mathrm{FWHM}}$, where δT_{FWHM} is determined by fitting the magnetic entropy curves with a Gaussian function. The RCP value is about 74.5 J kg^{-1} at 1 T and increases to about 264.5 J kg^{-1} at 9 T magnetic field for the $x = 0.25$ sample, as shown in Fig. 4(f). This is significantly higher than the value for the $x = 0$ sample, see Figs. 4(e) and 4(f). Therefore, the doped Co_2-based Heusler alloys are potential candidates for MCE applications as they show a second-order magnetic phase transition, their T_C can be tuned systematically to the desired temperature range and the RCP can be improved significantly through Ti doping [25,30].

For a further understanding of the magnetic interactions in these Heusler alloys, we did choose the $x = 0.25$ sample due to its relatively sharp magnetic phase transition and performed a critical behavior analysis in detail. For this purpose, the critical exponents β and γ can be determined using the following equations:

$$M_S(T) = M_0(-\epsilon)^{\beta}, \quad \epsilon < 0, T < T_C, \tag{2}$$

$$\chi_0^{-1} = (h_0/M_0)(\epsilon)^{\gamma}, \quad \epsilon > 0, T > T_C, \tag{3}$$

where $\epsilon = [(T\text{-}T_C)/T_C]$ is the reduced temperature, h_0/M_0 is the critical amplitude, and the exponents β and γ are related to the saturation magnetization $M_S(T)$ and the inverse initial magnetic susceptibility χ_0^{-1}, respectively [67]. The values of the critical exponents can give an idea about the different types of magnetic interactions present in the system. Therefore, we have used different theoretical models for modified Arrot plots, where we have applied different initial values for β and γ for the mean-field model (0.5, 1), the 3D Heisenberg model (0.365, 1.386), the Ising model (0.325, 1.24), and the tricritical model (0.25, 1). The corresponding $M^{1/\beta}$ was plotted versus $(H/M)^{1/\gamma}$ based on the Arrott-Noakes equation of state [67] for the $x = 0.25$ sample (data not shown here). For the best fit model, the plot should have straight and parallel lines in the high magnetic field region. We have fitted the curves in the high field region with the straight line and the line which passes through origin corresponds to the T_C value. Moreover, to determine best fit model, we have defined the normalized slope as $S(T)/S(T_C)$, where $S(T)$ is the slope of $M^{1/\beta}$ vs $(H/M)^{1/\gamma}$ at the temperature T and $S(T_C)$ is the slope at T_C. Figure 5(a) shows the normalized slope as a function of temperature for the $x = 0.25$ sample, fitted for the modified Arrott plots for the different models. The value of the normalized slope is found to be close to one, which indicates the mean-field model as the best fit model. The calculation of exact value of the critical exponents is an iterative method [68], where we use Eqs. (2) and (3) to obtain M_S (T, 0) and $\chi_0^{-1}(T, 0)$ at zero field from the linear extrapolation of a straight line fit of the high field region. We start with the initial values of $\beta = 0.5$ and $\gamma = 1$ for the mean-field model and fitted the curves of $M^{1/\beta}$ vs $(H/M)^{1/\gamma}$ using Eqs. (2) and (3), which gives stable values for the critical exponents, i.e., $\beta = 0.496$, $\gamma = 1.318$ for the $x = 0.25$ sample, as shown in Fig. 5(b). Now we use these values of β and γ and the fit shows straight lines in the high field region. However, the lines

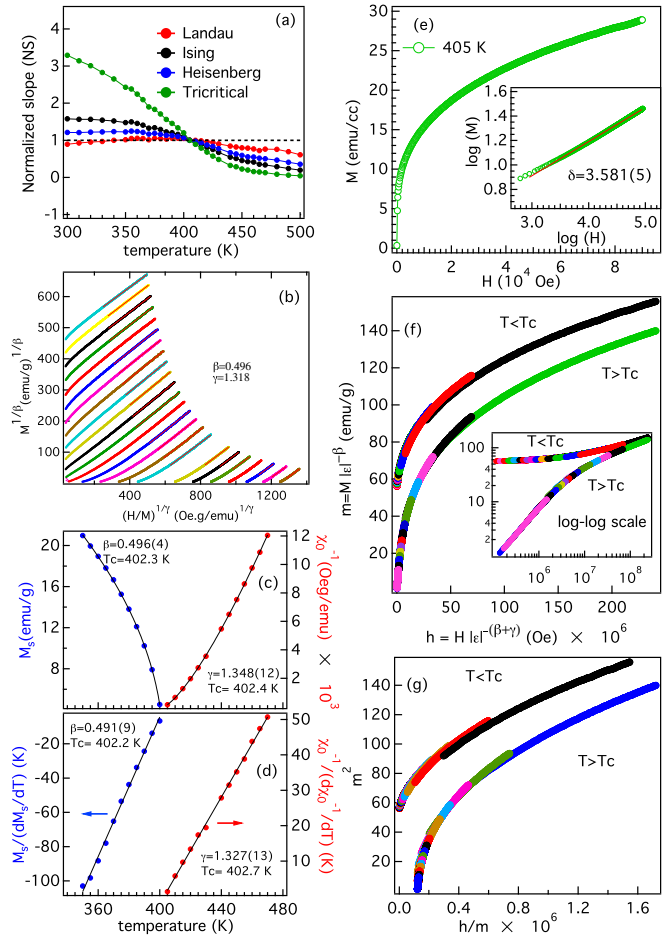

FIG. 5. Critical behavior analysis of $Co_2Cr_{0.75}Ti_{0.25}Al$ sample: (a) The temperature dependence of normalized slope (NS) of four different models, (b) modified Arrot plot $M^{1/\beta}$ vs $(H/M)^{1/\gamma}$ of the isotherms, (c) the plot of M_S (left axis) and χ_0^{-1} (right axis), and (d) the Kouvel-Fisher plot of M_S (left axis) and χ_0^{-1} (right axis) as a function of temperature. (e) The M vs H curve along with the log-log scale plot in the inset. (f) The renormalized magnetization (m) plotted as a function of renormalized field h and (g) the plot in the form of m^2 vs h/m.

are not perfectly straight probably due to a complex domain structure in the low field region. Furthermore, we have plotted M_S and χ_0^{-1} as a function of temperature from Fig. 5(b) by taking the slope values on $M^{1/\beta}$ and $(H/M)^{1/\gamma}$, respectively. In Fig. 5(c), the fit of a power-law function following Eqs. (2) and (3) gives values of $\beta = 0.496(4)$ and $\gamma = 1.348(12)$ for the $x = 0.25$ sample, which are close to the one obtained from Fig. 5(b). This confirms the reliability of the obtained critical exponents β and γ.

It is important to further verify the accuracy of these critical exponents obtained from the modified Arrott plot. Therefore, Eqs. (2) and (3) have been expressed following the Kouvel-Fisher method, as below:

$$M_S(T)/[dM_S(T)/dT] = \beta^{-1}(T - T_C), \tag{4}$$

$$\chi_0^{-1}(T)/[d\chi_0^{-1}(T)/dT] = \gamma^{-1}(T - T_C), \tag{5}$$

$$\log M(H, T_C) = \delta^{-1}\log H, \tag{6}$$

where δ corresponds to the critical magnetization at T_C. The critical exponents β and γ have been calculated from Eqs. (4) and (5), respectively. The slope of the straight line fit to the plots of $M_S\ (dM_S/dT)^{-1}$ and $\chi_0^{-1}\ (d\chi_0^{-1}/dT)^{-1}$ as a function of temperature, as shown in Fig. 5(d), gives the values of $1/\beta$ and $1/\gamma$. The value of δ is obtained using Eq. (6), where the slope of a straight line fit of log(M) vs. log(H) curve at T_C gives $1/\delta$ [see Fig. 5(e)]. Using Eqs. (4), (5), and (6), the obtained values are $\beta = 0.491(9)$, $\gamma = 1.327(13)$, and $\delta = 3.581(5)$ for the $x = 0.25$ sample. These values are quite close to those reported recently for similar Heusler compound Co_2TiGe by Roy *et al.* in Ref. [37] and are comparable to the theoretical values [69]. Furthermore, we have used the Widom scaling relation $\gamma - \beta(\delta - 1) = 0$ to validate the accuracy of the δ value, which was found to be in agreement with the one obtained from the critical isotherm, the Kouvel-Fisher method, and the modified Arrott plot.

The obtained values of β and γ suggest two types of magnetic interactions in the system. Below T_C, the estimated β value is close to the mean-field model, which indicates long-range magnetic interactions, while the value of γ deviates from mean field toward the 3D Heisenberg model above T_C, which suggests the presence of the local magnetic interactions. This behavior is in agreement with a recent study on Co_2TiGe [37] as well as other intermetallic compounds [34], where the critical exponents suggest the presence of complex magnetic interactions. Therefore, the values of the critical exponents offer the opportunity to check the scaling equation of the magnetic state, which can be performed as follows:

$$M(H, \epsilon) = \epsilon^{\beta} f_{\pm}\left(\frac{H}{\epsilon^{\beta+\gamma}}\right), \tag{7}$$

where f_- and f_+ are regular analytical functions below and above T_C, respectively. This scaling equation of state describes the relationship between M (H, ϵ), H and T_C. Following Eq. (7), the scaled magnetization $m = \epsilon^{-\beta} M(H, \epsilon)$ as a function of scaled field $h = \epsilon^{-(\beta+\gamma)} H$ should show two distinct branches across the Curie temperature T_C. Therefore, in Fig. 5(f), we show the scaled value of m versus the scaled value of h. This clearly demonstrates the expected behavior and is a further validation of the above determined values of critical exponents $(\beta,\ \gamma)$ and T_C. The same plot in log-log scale is shown in the inset of Fig. 5(f). The splitting of m^2 vs h/m into two branches across the T_C also indicates the reliability of the determined exponents and T_C as depicted in Fig. 5(g).

Notably, the values of the critical exponents obtained by the detailed analysis for the $x = 0.25$ sample do not follow any conventional universality class and predict that the system deviates from the mean field toward the 3D Heisenberg model, i.e., long-range type as well as local magnetic interactions below and above T_C, respectively. This indicates that the nature and range of complex spin interactions are playing a crucial role in determining the magnetic properties of this compound. It has been reported that isotropic exchange interactions between spins can give rise to extended spin interactions [25,37,70], which we can represent in terms of the exchange distance $J(r)$. In case of long-range exchange interactions, $J(r)$ decays as $J(r) \approx r^{-(D+\sigma)}$; whereas short-range interactions decay according to $J(r) \approx e^{-r/b}$ where r is the distance, D is the lattice dimensionality, and b is a specific scaling factor [70]. Here, the crucial parameter is σ, which determines the interaction range and depending on its value, i.e., if $\sigma < 1.5$ or > 2 indicates the presence of long range or short range spin interactions, respectively. Therefore, we have calculated the σ value following the renormalization group approach where the susceptibility exponent γ can be expressed by the equation below [70,71]:

$$\gamma = 1 + \frac{4}{D}\frac{d+2}{d+8}\Delta\sigma + \frac{8(d+2)(d-4)}{D^2(d+8)^2} \times \left[1 + \frac{2G\left(\frac{D}{2}\right)(7d+20)}{(d-4)(d+8)}\right]\Delta\sigma^2, \tag{8}$$

where d is the spin dimensionality and $\Delta\sigma$ and $G(\frac{D}{2})$ can be defined as $\sigma - \frac{D}{2}$ and $3 - \frac{1}{4}(\frac{D}{2})^2$, respectively. As discussed above, the value of σ can give an idea of the length scale of the spin interactions. Therefore, σ is calculated using the above equation and the experimental value of $\gamma = 1.348$. By considering $\{D : d\}$=$\{3 : 3\}$, we found a σ value of about 1.85. We note here that for a value of σ between 1.5 and 2, the system possesses extended type spin interactions other than the existing universality classes. With the obtained value of σ, the other critical exponents can be calculated using the expressions $\upsilon = \gamma/\sigma$, $\alpha = 2 - \upsilon d$, $\beta = (2 - \alpha - \gamma)/2$, and $\delta = 1 + \gamma/\beta$, where υ is the exponent of the correlation length. By taking $\sigma = 1.85$, the critical exponents are determined to be $\beta = 0.404$ and $\delta = 4.337$, which deviate from the experimental values (as discussed above for the $x = 0.25$ sample) and further suggests the presence of complex magnetic interactions in the sample. Interestingly, our study indicates that the long-range exchange interactions dominate below T_C, which are coupled with the 3D Heisenberg-type short-range spin interactions across the magnetic phase transition [37]. This motivates us for future investigations to understand its origin.

IV. CONCLUSIONS

The structural and magnetocaloric properties of $Co_2Cr_{1-x}Ti_xAl$ Heusler alloys have been investigated using XRD, ND, and magnetization measurements. The Rietveld refinement of the XRD data indicates an increase of the lattice parameter and unit cell volume with Ti substitution. We observed a second-order phase transition from PM to FM where the Curie temperature systematically increases from 330 K for the $x = 0$ sample to 445 K for the $x = 0.5$ sample. The neutron powder-diffraction data of the $x = 0$ sample taken across the magnetic phase transition in a large temperature range confirm the structural stability. Further, the magnetic moment of the $x = 0$ sample is found to be 1.45 μ_B/f.u. from magnetization measurements, which is in good agreement with the value of 1.35 ± 0.05 μ_B/f.u. extracted by the Rietveld analysis of the neutron powder-diffraction pattern measured at 4 K. By analyzing the temperature-dependent ND data for the $x = 0$ sample, we find that the change in the magnetic intensity of the most intense Bragg peak (220) is consistent with the increase in the magnetic moment with temperature. Moreover,

an enhancement in the change in the magnetic entropy ΔS_m and the RCP was observed for the $x = 0.25$ sample. Furthermore, our study reveals the presence of long-range ferromagnetic ordering below T_C, which deviates toward short 3D Heisenberg-type spin interactions above T_C based on the analysis of the critical behavior across the second-order phase transition with the extracted exponents values of $\beta \approx 0.496(4)$, $\gamma \approx 1.348(12)$, and $\delta \approx 3.71(5)$ for the $x = 0.25$ sample, which is further supported by the interaction range ($\sigma = 1.85$) analysis.

ACKNOWLEDGMENTS

This work was financially supported by the BRNS through a DAE Young Scientist Research Award to R.S.D. with Project Sanction No. 34/20/12/2015/BRNS. P.N. and G.D.G. thank the MHRD, India for fellowship through IIT Delhi. Authors acknowledge the physics department, IIT Delhi and UGC-DAE CSR, Mumbai center for XRD and magnetic measurements. P.N., G.D.G., and R.S.D. thank Sanjay Singh for help in ND data analysis and useful discussions. We thank V. Siruguri for support in performing the magnetic measurements. R.S.D. also gratefully acknowledges the financial support from the Department of Science & Technology (DST), India through Indo-Australia Early and Mid-Career Researchers (EMCR) fellowship, administered by INSA (Sanction Order No. IA/INDO-AUST/F-19/2017/1887) for performing the neutron measurements at ANSTO, Australia. C.U. thanks the Australian Research Council (ARC) for support through Discovery Grant No. DP160100545.

[1] C. Felser, and A. Hirohata, *Heusler Alloys: Properties, Growth, Applications*, Springer Series of Materials Science Vol. 222 (Springer International Publishing, Switzerland, 2016).

[2] I. Galanakis, P. H. Dederichs, and N. Papanikolaou, Slater-Pauling behavior and origin of the half-metallicity of the full-Heusler alloys, Phys. Rev. B **66**, 174429 (2002).

[3] M. Zhang, Z. Liu, H. Hu, G. Liu, Y. Cui, J. Chen, G. Wu, X. Zhang, and G. Xiao, Is Heusler compound Co_2CrAl a half-metallic ferromagnet: Electronic band structure, and transport properties, J. Mag. Magn. Mater. **277**, 130 (2004).

[4] Y. Miura, M. Shirai, and K. Nagao, *Ab initio* study on stability of half-metallic Co-based full-Heusler alloys, J. Appl. Phys. **99**, 08J112 (2006).

[5] S. Husain, S. Akansel, A. Kumar, P. Svedlindh, and S. Chaudhary, Growth of Co_2FeAl Heusler alloy thin films on Si(100) having very small Gilbert damping by ion beam sputtering, Sci. Rep. **6**, 28692 (2016).

[6] A. Husmann, and L. J. Singh, Temperature dependence of the anomalous Hall conductivity in the Heusler alloy Co_2CrAl, Phys. Rev. B **73**, 172417 (2006).

[7] T. Block, C. Felser, G. Jakob, J. Ensling, B. Mühling, P. Gütlich, and R. J. Cava, Large negative magnetoresistance effects in $Co_2Cr_{0.6}Fe_{0.4}Al$, J. Solid State Chem. **176**, 646 (2003).

[8] S. Wurmehl, G. H. Fecher, H. C. Kandpal, V. Ksenofontov, C. Felser, and H. Lin, Investigation of Co_2FeSi: The Heusler compound with highest Curie temperature and magnetic moment, Appl. Phys. Lett. **88**, 032503 (2006).

[9] J. Kübler, G. H. Fecher, and C. Felser, Understanding the trend in the Curie temperatures of Co_2-based Heusler compounds: *Ab initio* calculations, Phys. Rev. B **76**, 024414 (2007).

[10] E. Sasioglu, L. M. Sandratskii, P. Bruno, and I. Galanakis, Exchange interactions and temperature dependence of magnetization in half-metallic Heusler alloys, Phys. Rev. B **72**, 184415 (2005).

[11] P. Nehla, C. Ulrich, and R. S. Dhaka, Investigation of the structural, electronic, transport and magnetic properties of Co_2FeGa Heusler alloy nanoparticles, J. Alloys Compd. **776**, 379 (2019).

[12] D. Rani, J. Kangsabanik, K. G. Suresh, N. Patra, D. Bhattacharyya, S. N. Jha, and A. Alam, Origin of Local Atomic Order and Disorder in $Co_2Fe_{1-x}Cr_xSi$ Heusler Alloys: Theory and Experiment, Phys. Rev. Appl. **10**, 054022 (2018).

[13] C. J. Palmstrom, Heusler compounds and spintronics, Prog. Crystal Growth Charact. Mater. **62**, 371 (2016).

[14] G. H. Fecher, H. C. Kandpal, S. Wurmehl, C. Felser, and G. Schnhöense, Slater-Pauling rule and Curie temperature of Co_2–based Heusler compounds, J. Appl. Phys. **99**, 08J106 (2006).

[15] R. Y. Umetsu, K. Kobayashi, A. Fujita, K. Oikawa, R. Kainuma, and K. Ishida, Half-metallic properties of $Co_2(Cr_{1-x}Fe_x)Ga$ Heusler alloys, Phys. Rev. B **72**, 214412 (2005).

[16] M. A. Zagrebin, V. V. Sokolovskiy, V. D. Buchelnikov, and O. O. Pavlukhina, Effect of structural disorder on the ground state properties of Co_2CrAl Heusler alloy, Physica B: Cond. Matter **519**, 82 (2017).

[17] Y. V. Kudryavtsev, V. N. Uvarov, V. A. Oksenenko, Y. P. Lee, J. B. Kim, Y. H. Hyun, K. W. Kim, J. Y. Rhee, and J. Dubowik, Effect of disorder on various physical properties of Co_2CrAl Heusler alloy films: Experiment and theory, Phys. Rev. B **77**, 195104 (2008).

[18] Q. F. Li, H. F. Zhao, and L. Wang, An *ab initio* study of CoCr(V) disorder effects on the electronic structure and magnetic properties of $Co_2Cr_{1-x}V_xAl$, Solid. State Commun. **150**, 109 (2010).

[19] Y. Miura, K. Nagao, and M. Shirai, Atomic disorder effects on half-metallicity of the full-Heusler alloys $Co_2(Cr_{1-x}Fe_x)Al$: A first-principles study, Phys. Rev. B **69**, 144413 (2004).

[20] M. D. Mukadam, S. Roy, S. S. Meena, P. Bhatt, and S. M. Yusuf, Quantification of site disorder and its role on spin polarization in the nearly half-metallic Heusler alloy NiFeMnSn, Phys. Rev. B **94**, 214423 (2016).

[21] Y. Feng, H. Chen, H. Yuan, Y. Zhou, and X. Chen, The effect of disorder on electronic and magnetic properties of quaternary Heusler alloy CoFeMnSi with LiMgPbSb-type structure, J. Magn. Magn. Mater **378**, 7 (2015).

[22] H. C. Kandpal, V. Ksenofontov, M. Wojcik, R. Seshadri, and C. Felser, Electronic structure, magnetism and disorder in the Heusler compound Co_2TiSn, J. Phys. D: Appl. Phys. **40**, 1587 (2007).

[23] S. C. Lee, T. D. Lee, P. Blaha, and K. Schwarz, Magnetic and half-metallic properties of the full-Heusler alloys Co_2TiX ($X =$ Al, Ga; Si, Ge, Sn; Sb), J. Appl. Phys. **97**, 10C307 (2005).

[24] Y. Feng, and X. Xu, Tunable magnetism and half metallicity in Ti-doped Heusler alloy Co_2CrAl: First-principles calculations, J. Supercond. Nov. Magn. **31**, 1827 (2017).

[25] P. Nehla, V. K. Anand, B. Klemke, B. Lake, and R. S. Dhaka, Magnetocaloric properties and critical behavior of $Co_2Cr_{1-x}Mn_xAl$ Heusler alloys, arXiv:1907.06114v1.

[26] S. Mizusaki, T. Ohnishi, T. C. Ozawa, Y. Noro, M. Itou, Y. Sakurai, and Y. Nagata, Spin-polarized itinerant electrons in Co-based Heusler compounds investigated by magnetic Compton scattering, J. Appl. Phys. **111**, 063915 (2012).

[27] T. Graf, G. H. Fecher, J. Barth, J. Winterlik, and C. Felser, Electronic structure and transport properties of the Heusler compound Co_2TiAl, J. Phys. D: Appl. Phys. **42**, 084003 (2009).

[28] E. DiMasi, M. C. Aronson, and B. R. Coles, Pressure dependence of the Curie temperature of Co_2TiAl, Phys. Rev. B **47**, 14301 (1993).

[29] S. Singh, L. Caron, S. W. D'Souza, T. Fichtner, G. Porcari, S. Fabbrici, C. Shekhar, S. Chadov, M. Solzi, and C. Felser, Large magnetization and reversible magnetocaloric effect at the second-order magnetic transition in Heusler materials, Adv. Mater. **28**, 3321 (2016).

[30] J. Panda, S. N. Saha, and T. K. Nath, Critical behavior and magnetocaloric effect in $Co_{50-x}Ni_xCr_{25}Al_{25}$ ($x = 0$ and 5) full Heusler alloy system, J. Alloys Compd. **644**, 930 (2015).

[31] V. Franco, A. Conde, V. K. Pecharsky, and K. A. Jr. Gschichneidner, Field dependence of the magnetocaloric effect in Gd and $(Er_{1-x}Dy_x)Al_2$: Does a universal curve exist? Eur. Phys. Lett. **79**, 47009 (2007).

[32] E. Bruck, O. Tegus, D. T. C. Thanh, and K. H. J. Buschow, Magnetocaloric refrigeration near room temperature (invited), J. Mag. Magn. Mater. **310**, 2793 (2007).

[33] F. X. Hu, B. G. Shen, and J. R. Sun, Magnetic entropy change in $Ni_{51.5}Mn_{22.7}Ga_{25.8}$ alloy, Appl. Phys. Lett. **76**, 3460 (2000).

[34] M. Halder, S. M. Yusuf, and A. K. Nigam, Magnetocaloric effect and its implementation in critical behavior study of $Mn_4FeGe_{3-x}Si_x$ intermetallic compounds, J. Appl. Phys. **110**, 113915 (2011).

[35] B. M. Wang, L. Wang, Y. Liu, and B. C. Zhao, A second-order ferromagnetic transition in the martensitic state of $Ni_{49.5}Mn_{32.5}Cu_4Sn_{14}$: A critical behavior study, J. Appl. Phys. **105**, 023913 (2009).

[36] K. R. Kumar, H. S. Nair, B. N. Sahu, S. Xhakaza, and A. M. Strydom, Large magntocaloric effect and critical behavior analysis in Gd_2Cu_2In, Euro Phys. Lett. **122**, 17003 (2018).

[37] S. Roy, N. Khan, R. Singha, A. Pariari, and P. Mandal, Complex exchange mechanism driven ferromagnetism in half-metallic Heusler Co_2TiGe: Evidence from critical behavior, Phys. Rev. B **99**, 214414 (2019).

[38] A. J. Studer, M. E. Hagen, and T. J. Noakes, Wombat: The high-intensity powder diffractometer at the OPAL reactor, Physica B **385-386**, 1013 (2006).

[39] K.-D. Liss, B. Hunter, M. Hagen, T. Noakes, and S. Kennedy, Echidna–the new high-resolution powder diffractometer being built at OPAL, Physica B **385-386**, 1010 (2006).

[40] M. Avdeev and J. R. Hester, ECHIDNA: A decade of high-resolution neutron powder diffraction at OPAL, J. Appl. Cryst. **51**, 1597 (2018)

[41] J. Rodriguez-Carvajal, Recent advances in magnetic structure determination by neutron powder diffraction, Physica B **192**, 55 (1993).

[42] See Supplemental Material at http://link.aps.org/supplemental/10.1103/PhysRevB.100.144444 for further information about x-ray diffraction (for sample characterization) and neutron diffraction (high resolution from ECHIDNA and in large temperature range from WOMBAT) data.

[43] A. D. Svyazhin, E. I. Shreder, V. I. Voronin, I. F. Bergera, and S. E. Danilov, Atomic disorder and the magnetic, electrical, and optical properties of a Co_2CrAl Heusler alloy, J. Exp. Theor. Phys. **116**, 452 (2013).

[44] H. J. Elmers, G. H. Fecher, D. Valdaitsev, S. A. Nepijko, A. Gloskovskii, G. Jakob, G. Schönhense, S. Wurmehl, T. Block, C. Felser, P.-C. Hsu, W.-L. Tsai, and S. Cramm, Element-specific magnetic moments from core-absorption magnetic circular dichroism of the doped Heusler alloy $Co_2Cr_{0.6}Fe_{0.4}Al$, Phys. Rev. B **67**, 104412 (2003).

[45] T. Block, M. J. Carey, B. A. Gurney, and O. Jepsen, Band-structure calculations of the half-metallic ferromagnetism and structural stability of full- and half-Heusler phases, Phys. Rev. B **70**, 205114 (2004).

[46] C. Felser, B. Heitkamp, F. Kronast, D. Schmitz, S. Cramm, H. A. Dürr, H.-J. Elmers, G. H. Fecher, S. Wurmehl, T. Block, D. Valdaitsev, S. A. Nepijko, A. Gloskovskii, G. Jakob, G. Schönhense, and W. Eberhardt, Investigation of a novel material for magnetoelectronics: $Co_2Cr_{0.6}Fe_{0.4}Al$, J. Phys.: Condens. Matter **15**, 7019 (2003).

[47] I. Galanakis, Orbital magnetism in the half-metallic Heusler alloys, Phys. Rev. B **71**, 012413 (2005).

[48] W. Zhu, D. Wu, B. Zhao, Z. Zhu, X. Yang, Z. Zhang, and Q. Y. Jin, Correlations between structural and magnetic properties of Co_2FeSi Heusler-alloy thin films, Phys. Rev. Appl. **8**, 034012 (2017).

[49] M. Halder, S. M. Yusuf, A. Kumar, A. K. Nigam, and L. Keller, Crossover from antiferromagnetic to ferromagnetic ordering in the semi-Heusler alloys $Cu_{1-x}Ni_xMnSb$ with increasing Ni concentration, Phys. Rev. B **84**, 094435 (2011).

[50] K. R. Kumar, N. H. Kumar, P. D. Babu, S. Venkatesh, and S. Ramakrishnan, Investigation of atomic anti-site disorder and ferrimagnetic order in the half-metallic Heusler alloy Mn_2VGa, J. Phys.: Condens. Matter **24**, 336007 (2012).

[51] R. Y. Umetsu, K. Kobayashib, R. Kainuma, Y. Yamaguchi, K. Ohoyama, A. Sakuma, and K. Ishida, Powder neutron diffraction studies for the $L2_1$ phase of Co_2YGa (Y = Ti, V, Cr, Mn and Fe) Heusler alloys, J. Alloy Compd. **499**, 1 (2010).

[52] M. P. Raphael, B. Ravel, Q. Huang, M. A. Willard, S. F. Cheng, B. N. Das, R. M. Stroud, K. M. Bussmann, J. H. Claassen, and V. G. Harris, Presence of antisite disorder and its characterization in the predicted half-metal Co_2MnSi, Phys. Rev. B **66**, 104429 (2002).

[53] P Lázpita, J. M. Barandiarán, J. Gutiérrez, J. Feuchtwanger, V. A. Chernenko, and M. L. Richard, Magnetic moment and chemical order in off-stoichiometric Ni–Mn–Ga ferromagnetic shape memory alloys, New J. Phys. **13**, 033039 (2013).

[54] B. Ravel, M. P. Raphael, V. G. Harris, and Q. Huang, EXAFS and neutron diffraction study of the Heusler alloy Co_2MnSi, Phys. Rev. B **65**, 184431 (2002).

[55] X. Yan, A. Grytsiv, P. Rogl, V. Pomjakushin, and M. Palm, The Heusler phase $Ti_{25}(Fe_{50-x}Ni_x)Al_{25}$ ($0 \leqslant x \leqslant 50$); structure and constitution, J. Phase Equilib. Diffus. **29**, 500 (2008).

[56] M. Inagaki, H. Furuhashi, T. Ozeki, H. Mugishima, and S. Naka, Integrated intensity changes for crystalline powers by griding and compression–changes in effective temperature factor, J. Mater. Sci. **6**, 1520 (1971).

[57] M. Taheri, F. S. Razavi, Z. Yamani, R. Flacau, P. G. Reuvekamp, A. Schulz, and R. K. Kremer, Magnetic structure, magnetoelastic coupling, and thermal properties of $EuCrO_3$ nanopowders, Phys. Rev. B **93**, 104414 (2016).

[58] M. Reehuis, C. Ulrich, A. Maljuk, C. Niedermayer, B. Ouladdiaf, A. Hoser, T. Hofmann, and B. Keimer, Neutron diffraction study of spin and charge ordering in $SrFeO_{3-\delta}$, Phys. Rev. B **85**, 184109 (2012).

[59] T. D. Shen, R. B. Schwarz, J. Y. Coulter, and J. D. Thompson, Magnetocaloric effect in bulk amorphous $Pd_{40}Ni_{22.5}Fe_{17.5}P_{20}$ alloy, J. Appl. Phys. **91**, 5240 (2002).

[60] J. Y. Law, V. Franco, L. M. Moreno-Ram Õrez, A. Conde, D. Y. Karpenkov, I. Radulov, K. P. Skokov, and O. Gutfleisch, A quantitative criterion for determining the order of magnetic phase transitions using the magnetocaloric effect, Nat. Commun. **9**, 2680 (2018).

[61] V. Franco, J. S. Blazquez, and A. Conde, New type of magnetocaloric effect: Implications on low-temperature magnetic refrigeration using an Ericsson cycle, Appl. Phys. Lett. **89**, 222512 (2006).

[62] M. H. Phan, V. Franco, A. Chaturvedi, S. Stefanoski, G. Nolas, and H. Srikanth, Origin of the magnetic anomaly and tunneling effect of europium on the ferromagnetic ordering in $Eu_{8-x}Sr_xGa_{16}Ge_{30}$ ($x = 0, 4$) type-I clathrates, Phys. Rev. B **84**, 054436 (2011).

[63] V. Franco, R. Caballero-Flores, A. Conde, Q. Y. Dong, and H. W. Zhang, The influence of a minority magnetic phase on the field dependence of the magnetocaloric effect, J. Magn. Magn. Mater. **321**, 1115 (2009).

[64] C. Marcela Bonilla, J. Herrero-Albillos, F. Bartolome, L. M. Garcia, M. Parra-Borderias, and V. Franco, Universal behavior for magnetic entropy change in magnetocaloric materials: An analysis on the nature of phase transitions, Phys. Rev. B **81**, 224424 (2010).

[65] V. Franco, A. Conde, J. M. Romero-Enrique, and J. S. Blazquez, A universal curve for the magnetocaloric effect: An analysis based on scaling relations, J. Phys.: Condens. Matter **20**, 285207 (2008).

[66] Q. Dong, H. Zhang, J. Sun, B. Shen, and V. Franco, A phenomenological fitting curve for the magnetocaloric effect of materials with a second-order phase transition, J. Appl. Phys. **103**, 116101 (2008).

[67] A. Arrott and J. Noakes, Approximate Equation of State for Nickel Near its Critical Temperature, Phys. Rev. Lett. **19**, 786 (1967).

[68] L. Zhang, B. S. Wang, Y. P. Sun, P. Tong, J. Y. Fan, C. J. Zhang, L. Pi, and Y. H. Zhang, Critical behavior in the antiperovskite ferromagnet $AlCMn_3$, Phys. Rev. B **85**, 104419 (2012).

[69] S. N. Kaul, Static critical phenomena in ferromagnetics with quenched disorder, J. Magn. Magn. Mater. **53**, 5 (1985).

[70] M. E. Fisher, S.-K. Ma, and B. Nickel, Critical Exponents for Long-Range Interactions, Phys. Rev. Lett. **29**, 917 (1972).

[71] M. E. Fisher, The renormalization group in the theory of critical behavior, Rev. Mod. Phys. **46**, 597 (1974).